Nuclear effects in neutrino and antineutrino charged-current quasielastic scattering at MINERvA kinematics

Nuclear effects in neutrino and antineutrino charged-current quasielastic scattering at MINERνA kinematics

G. D. Megias,[1,*] M. V. Ivanov,[2,3] R. González-Jiménez,[1] M. B. Barbaro,[4] J. A. Caballero,[1] T. W. Donnelly,[5] and J. M. Udías[2]

[1]*Departamento de Física Atómica, Molecular y Nuclear, Universidad de Sevilla, 41080 Sevilla, Spain*
[2]*Grupo de Física Nuclear, Departamento de Física Atómica, Molecular y Nuclear, Facultad de Ciencias Físicas, Universidad Complutense de Madrid, CEI Moncloa, Madrid E-28040, Spain*
[3]*Institute for Nuclear Research and Nuclear Energy, Bulgarian Academy of Sciences, Sofia 1784, Bulgaria*
[4]*Dipartimento di Fisica, Università di Torino and INFN, Sezione di Torino, Via P. Giuria 1, 10125 Torino, Italy*
[5]*Center for Theoretical Physics, Laboratory for Nuclear Science and Department of Physics, Massachusetts Institute of Technology, Cambridge, Massachusetts 02139, USA*

(Received 6 February 2014; published 5 May 2014)

We compare the charged-current quasielastic neutrino and antineutrino observables obtained in two different nuclear models, the phenomenological SuperScaling Approximation and the relativistic mean field approach, with the recent data published by the MINERνA Collaboration. Both models provide a good description of the data without the need of an *ad hoc* increase in the mass parameter in the axial-vector dipole form factor. Comparisons are also made with the MiniBooNE results, where different conclusions are reached.

DOI: 10.1103/PhysRevD.89.093002 PACS numbers: 25.30.Pt, 13.15.+g, 24.10.Jv

I. INTRODUCTION

The MINERνA Collaboration has recently measured differential cross sections for neutrino and antineutrino charged-current quasielastic (CCQE) scattering on a hydrocarbon target [1,2]. "Quasielastic" events are defined, in this case, as containing no mesons in the final state. The beam energy goes from 1.5 to 10 GeV and is peaked at $E_\nu \sim 3$ GeV. At lower energies $E_\nu \sim 0.7$ GeV, the MiniBooNE experiment has reported [3,4] CCQE cross sections that are higher than most theoretical predictions based on the impulse approximation (IA), leading to the suggestion that non-quasielastic (non-QE) processes induced by two-body currents may play a significant role in this energy domain [5–8]. These effects have sometimes been simulated, in the relativistic Fermi gas (RFG) framework, by a value of the nucleon axial-vector dipole mass $M_A = 1.35$ GeV [3,4], which is significantly larger than the standard value $M_A = 1.032$ GeV extracted from neutrino-deuterium quasielastic scattering. On the other hand, higher energy data from the NOMAD experiment ($E_\nu \sim 3$–100 GeV) are well accounted for by IA models [9]. The MINERνA experiment is situated in between these two energy regions, and its interpretation can therefore provide valuable information on the long-standing problem of assessing the role of correlations and meson exchange currents (MECs) in the nuclear dynamics [10–12].

In this paper we present results corresponding to two different nuclear models: the SuSA (SuperScaling Approximation) and the RMF (relativistic mean field) approach. Both have been extensively tested against existing QE electron scattering data over a wide energy range. The detailed description of these models can be found in our previous work (see, e.g., [13] and [14]). Here we just summarize their main features and address some improvements with respect to previous work.

II. RESULTS

SuSA [13] is based on the idea of using electron scattering data to predict CC neutrino cross sections: a phenomenological "superscaling function" $f(\psi)$, depending only on one "scaling variable" $\psi(q,\omega)$ and embodying the essential nuclear dynamics, can be extracted from QE longitudinal (e,e') data within a fully relativistic framework. This function is then multiplied by the appropriate charge-changing N $\to$ N ($n \to p$ for neutrino and $p \to n$ for antineutrino scattering) weak interaction cross sections to obtain the various response functions that contribute to the inclusive neutrino-nucleus cross section. On the one hand, the model gives a good representation of the purely nucleonic contributions to the existing QE electron scattering data, to the extent that quasielastic scattering can be isolated. On the other hand, it does not account for inelastic scattering and MECs, which are mainly seen in the transverse channel. For the former, the SuSA approach has been successfully extended to higher energies into the non-QE regime where inelastic contributions dominate [15]. The latter have been modeled using extensions of the RFG for two-body operators and typically cause 10%–20% scaling violations.

The model works well for high enough momentum and energy transfers, whereas in the low q and ω region (typically, $q \leq 400$ MeV/c and $\omega \leq 50$ MeV), it is

*megias@us.es

inadequate, and different approaches that account for Pauli blocking and collective nuclear excitations should be used. In the phenomenological SuSA approach, Pauli blocking effects are not trivial to implement and have been neglected so far in our previous applications of the model. In this work we introduce them using the procedure proposed in [16], which generalizes the simple RFG prescription—only valid for a steplike momentum distribution—to accommodate more realistic momentum distributions. In summary, the prescription consists in subtracting from the scaling function $f(\psi(\omega,q))$ its mirror function $f(\psi(-\omega,q))$: this, as argued in that reference, incorporates a correct blocking of unphysical excitations, which are then excluded in a more satisfactory way than through the *ad hoc* factor $[1-n(\mathbf{p}+\mathbf{q})/n(0)]$ commonly used in the literature. If applied to a non-Pauli-blocked version of the RFG, this procedure yields exactly the correct Pauli blocking for that model. Moreover, this method does not require the knowledge of the nucleon momentum distribution $n(p)$. Additionally, Coulomb corrections for the outgoing lepton are taken into account in the SuSA approach [13], and a phenomenological energy shift $E_{\text{shift}} = 20$ MeV is introduced in the scaling variable in order to reproduce the correct peak position of electron-scattering data [17].

In Fig. 1, Pauli blocking effects in the scaling function for different fixed values of the transferred momentum are shown. Pauli blocking effects are noticeable when $q <$ 250 MeV and the subtractions to the non-Pauli-blocked scaling function come mainly from $\omega < 50$ MeV.

The second model we consider is the RMF, where the nucleons' wave functions are, for both the bound and scattering states, solutions of the Dirac-Hartree equation in the presence of strong, energy-independent, real scalar-attractive and vector-repulsive potentials. The model fulfills dispersion relations and maintains the continuity equation [18]. In the RMF model, the nucleons are dynamically and strongly *off-shell*, and, as a consequence, the cross section is not factorized into a spectral function and an elementary lepton-nucleus cross section, as happens in other approaches [19]. In order to appreciate the effects of off-shellness on the RMF results, we also show results in which the spinors are put exactly on the mass shell, within the so-called effective momentum approach (EMA) [20].

Before entering into the comparison of fully folded results with the neutrino spectrum results, first in Fig. 2 the unfolded CCQE neutrino cross section at Minerva kinematics for a fixed neutrino energy of 3 GeV is presented and is evaluated within the RMF and SuSA models, with and without Pauli blocking. It can be seen that Pauli blocking softly decreases the cross section at low Q^2_{QE}, which is directly related to the higher contribution of the low q and ω kinematic region in this case. Note also that our theoretical results for a fixed E_ν value (near the peak of the flux) are in good agreement with the MINERνA data, as also observed in [21]. It is interesting to see that for $|Q^2_{QE}| > 0.2$ (GeV/c)^2 the RMF cross section is slightly higher than the SuSA results.

In Fig. 3 we display the flux-folded differential cross section $d\sigma/dQ^2_{QE}$ for both neutrino (upper panel) and antineutrino (lower panel) scattering off a hydrocarbon (CH) target as a function of the reconstructed four-momentum transfer squared (Q^2_{QE}), that is obtained in the same way as for the experiment, assuming an initial-state nucleon at rest with a constant binding energy, E_b, set to 34 MeV (30 MeV) in the neutrino (antineutrino) case. The cross sections are folded with the MINERνA ν_μ and $\bar{\nu}_\mu$ fluxes [1,2], and the nucleon's axial mass has the standard value $M_A = 1.032$ GeV. We observe that both SuSA and RMF models yield predictions in excellent agreement with

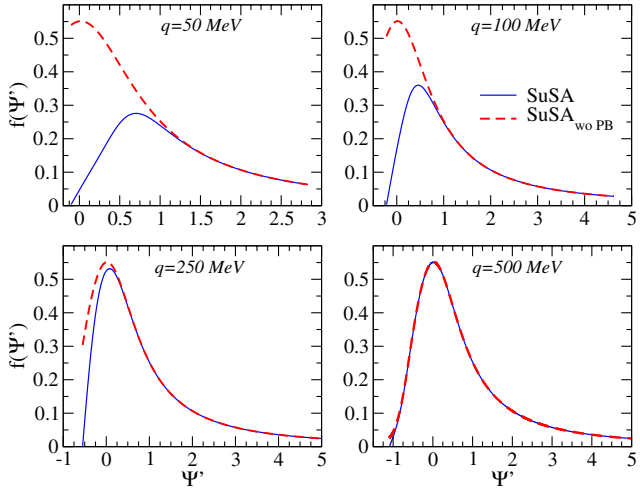

FIG. 1 (color online). Superscaling function versus ψ' at different q-fixed values and evaluated for the SuSA model with (SuSA) and without (SuSA$_{woPB}$) Pauli blocking.

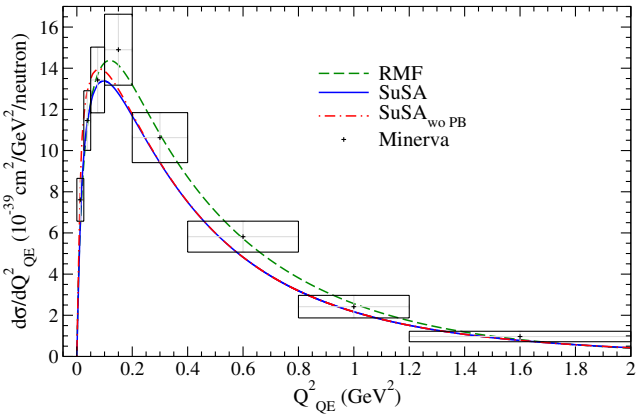

FIG. 2 (color online). Unfolded CCQE $\nu_\mu - {}^{12}$C scattering cross section per target nucleon as a function of Q^2_{QE} at fixed neutrino energy $E_\nu = 3$ GeV and evaluated in the RMF and in the SuSA (with and without Pauli blocking) models. MINERνA data are from [1,2].

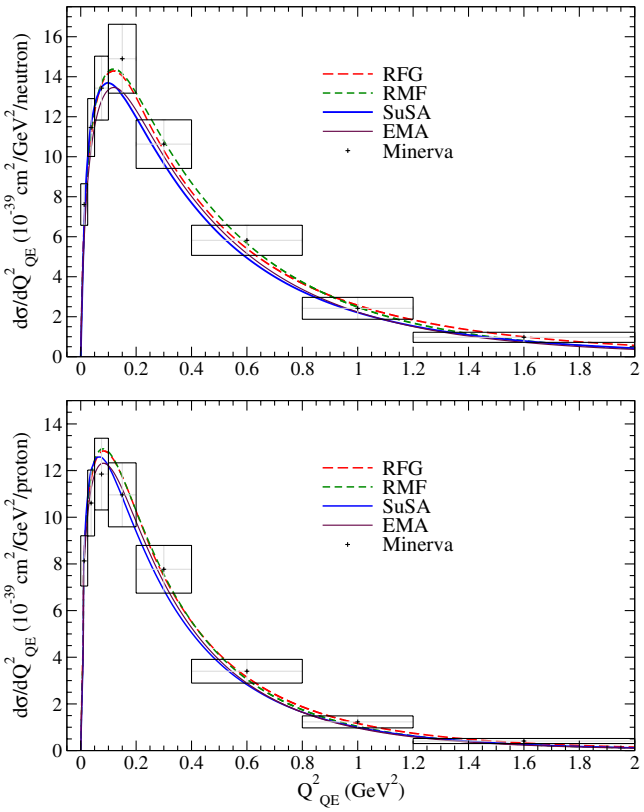

FIG. 3 (color online). Flux-folded CCQE $\nu_\mu - {}^{12}\mathrm{C}$ (upper panel) and $\bar{\nu}_\mu - \mathrm{CH}$ (lower panel) scattering cross section per target nucleon as a function of Q^2_{QE} and evaluated in the SuSA, RMF, and EMA models. MINERνA data are from [1,2].

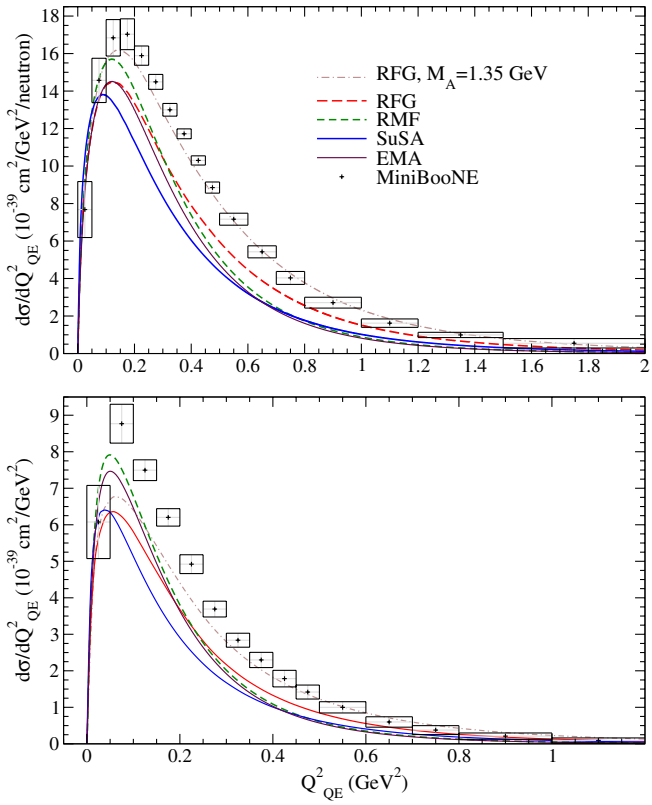

FIG. 4 (color online). Flux-folded CCQE $\nu_\mu - {}^{12}\mathrm{C}$ (upper panel) and $\bar{\nu}_\mu - {}^{12}\mathrm{C}$ (lower panel) scattering cross section per target nucleon as a function of Q^2_{QE} and evaluated in the SuSA, RMF, and EMA models and compared with MiniBooNE data [3,4]. The RFG model is shown for two values of the axial mass (see text for details).

the experimental data, leaving not much space for large effects of 2p2h contributions, although perhaps $\sim 10\%$ additional effects from MEC are acceptable. RMF results are slightly higher than the SuSA ones, an outcome already observed at MiniBooNE kinematics (see also Fig. 2), which is related to the lower component enhancement of the RMF spinors. Indeed, the EMA curves, where such off-shell effects are absent, lie closer to the SuSA results. The RFG model is also shown for reference. In the RFG calculation, we use the formalism of [22], assuming a Fermi momentum of 228 MeV/c and an energy shift of 20 MeV. This is not the same as the RFG modeling of GENIE [23] and NuWRO [24], which could explain the slight difference between our RFG results and the ones reported in [1,2]. Note that the RFG model with the standard value of the axial mass (red-dashed curve) also fits the data, being in very good agreement with the other approaches, in particular with RMF. Finally, the spread in the curves corresponding to the four models is less than 7% in the case of neutrinos and less than 5% in the case of antineutrinos (see the discussion below). The theoretical results presented here include the whole energy range for the neutrino. The experimentalists implement several cuts on the phase space of the data, such as restricting the kinematics to contributions from neutrino energies below 10 GeV. The impact of such a cut on the results we present here is smaller than 0.2%, in the worst case. In the experimental analysis, several cuts were imposed to the initial data sample to increase the ratio of true quasielastic events in the sample. The effect of these cuts has been incorporated into the efficiency factors of the experiment, and thus, the data have been corrected for them [25]. We apply no cuts to the theoretical results, as the data have been corrected for their effect.

For completeness we illustrate in Fig. 4 the differential cross section $d\sigma/dQ^2_{QE}$ corresponding to the MiniBooNE experiment. The same qualitative behavior among the models is observed here as for MINERνA kinematics. Namely, the SuSA approach provides the lowest cross section and RFG/RMF the highest one, and as already shown in the previous figure, the EMA curves come closer to SuSA. However, the spread among the different theoretical predictions is larger for MiniBooNE, about twice as much as for MINERνA. Further, in contrast to the MINERνA experiment, all models exhibit a different energy dependence and underestimate the MiniBooNE data, unless the axial mass in the dipole parameterization of the axial-vector form factor is significantly increased

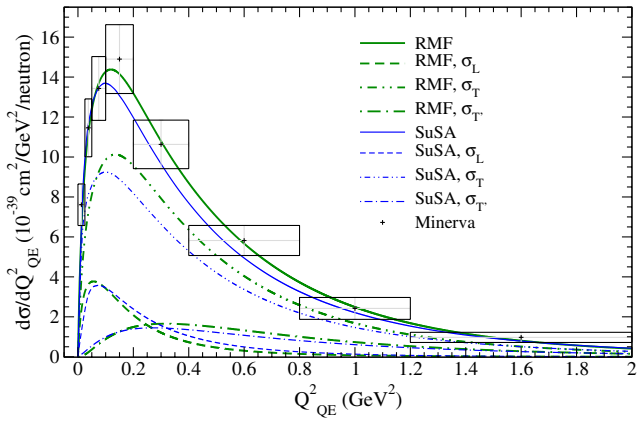

FIG. 5 (color online). Separated contributions of CCQE $\nu_\mu - {}^{12}\mathrm{C}$ $d\sigma/dQ^2_{QE}$ in the SuSA and RMF models.

(see the RFG curve for $M_A = 1.35$ GeV). Note also that the MiniBooNE Collaboration reproduces their $d\sigma/dQ^2_{QE}$ measurements by normalizing their RFG predictions ($M_A = 1.35$ GeV) to the observed total cross section. Moreover, although MiniBooNE data error bands are much smaller than the ones corresponding to MINERνA, the comparison between theory and data shows a clear difference between the two situations: whereas in the former (MiniBooNE) no model based on the IA is capable of reproducing the data, in the latter (MINERνA), the IA already provides a good description of data and the enlargement of the axial mass worsens this agreement.

In Fig. 5 we display the separate contributions of the longitudinal (L), transverse (T), and transverse-axial interference (T') channels to the differential cross section within the two models, SuSA and RMF, showing that the transverse response is dominant in the full range of Q^2_{QE}. As observed, the difference between the SuSA and RMF results is mostly linked to the T response. Moreover, the different role played by the interference T' response for neutrinos (constructive) and antineutrinos (destructive) explains the overall difference between SuSA and RMF curves for the cross section, being larger for neutrinos (Figs. 3 and 4).

It was shown in [9] that, even at *high* neutrino energies, *low* energy and momentum transfers play a crucial role in the CCQE cross section. To illustrate this point in the specific conditions of MINERνA, we display in Fig. 6 the neutrino cross section evaluated in the SuSA model by applying different cuts in q (upper panel) and ω (lower panel): it clearly appears that, even if the neutrino energy is as large as 3 GeV, the process is largely dominated by energy and momentum transfer, namely, $\omega < 50$ MeV, $q < 1000$ MeV. In Fig. 6 we also give the relative contribution to the cross section (expressed in percentage) attached to the different (q, ω) regions considered. Note how the relative fraction diminishes very significantly for increasing q, ω values.

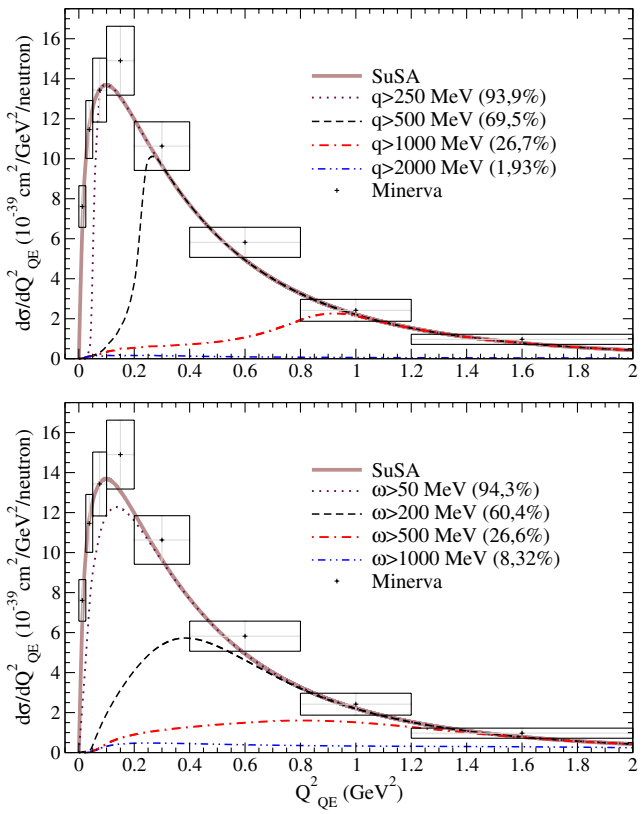

FIG. 6 (color online). Flux-folded CCQE $\nu_\mu - {}^{12}\mathrm{C}$ differential cross section per target nucleon evaluated excluding all contributions coming from transferred momentum (upper panel) and energy (lower panel) below some selected values, as indicated in the figure. MINERνA data are from [1,2]. The numbers in parentheses refer to the fraction of the total cross section corresponding to each curve.

In Table I we report the values of the total cross sections per nucleon integrated over the flux from 1.5 to 10 GeV for both neutrino and antineutrino scattering: the results corresponding to all models (RFG, SuSA, RMF, and EMA) are compatible with the experimental data within the error bars. The discrepancy between theory and data (central values) is at most of the order of ~9%–10% (SuSA/EMA), being reduced to ~2%–3% for RMF/RFG.

Finally, in Fig. 7 the data and models are shown versus Q^2_{QE} as a ratio to the GENIE [23] prediction, in the same way they are presented by the MINERνA Collaboration [1,2]. The ratio has the advantage of minimizing systematic uncertainties and better emphasizing the differences

TABLE I. Comparisons between the measured total cross section (per nucleon) after averaging over the flux and the results obtained with the RFG, SuSA, and RMF models.

Model	RFG	SuSA	RMF	EMA	Experimental
$\sigma_{\nu_\mu}(10^{-38}\ \mathrm{cm}^2)$	0.916	0.834	0.901	0.828	0.93 ± 0.12
$\sigma_{\bar{\nu}_\mu}(10^{-38}\ \mathrm{cm}^2)$	0.601	0.550	0.583	0.554	0.604 ± 0.083

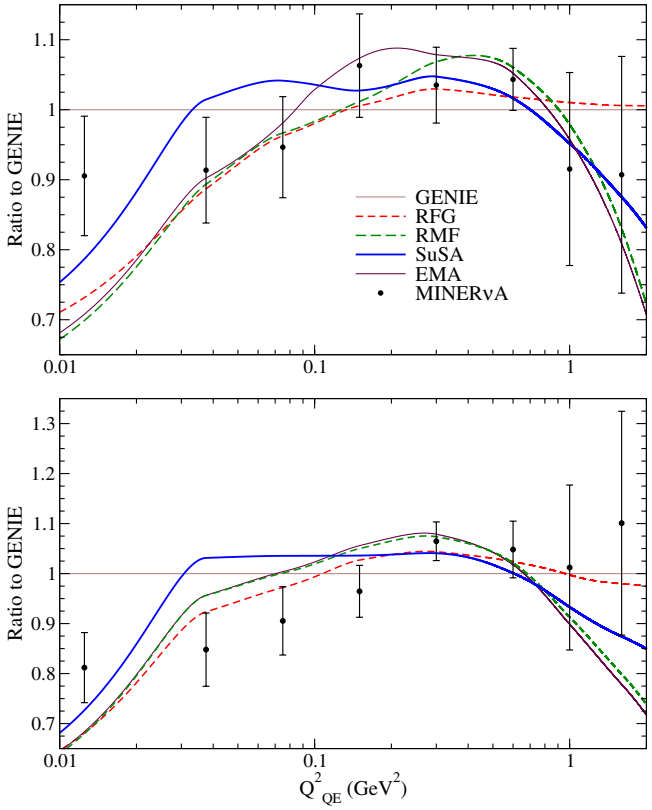

FIG. 7 (color online). The MINERνA data and models of Fig. 3 shown versus Q^2_{QE} as a ratio to the GENIE prediction. Upper panel: neutrino case. Lower panel: antineutrino case.

between various models. More specifically, the results are obtained by dividing each theoretical model and the experimental data by the GENIE result and normalizing these results to have the same total cross section across the range $Q^2 \in [0, 2]$ GeV^2 as GENIE has. As shown, all of the theoretical results, except SuSA, are within the error bars of all but the lowest Q^2 data for the neutrino ratio, while there is a slight overestimation in the central Q^2 data for the antineutrino case. Actually the SuSA curve departs from the other models for the lower three data points. Note however that the ratio is strongly affected by the above-mentioned normalization. Moreover, this is the region where the differential cross section reaches its maximum and changes its shape dramatically, which, in addition to the reduced size of the bins in this region, makes it difficult to compare accurately theory and data. For higher Q^2_{QE} the agreement of theory and data improves for neutrinos (upper panel) where all theoretical results lie within the data error bands except SuSA for Q^2_{QE} bins in the range $[0.025, 0.1]$ GeV^2. For antineutrinos theory lies above data for $Q^2 \in [0.025, 0.2]$ GeV^2. In all of the cases, neutrinos and antineutrinos, the differences between theoretical predictions are larger at the extreme Q^2_{QE} bins, being significantly reduced within the central values of Q^2_{QE} where the comparison with data is also much better.

TABLE II. Comparisons between the measured $d\sigma/dQ^2_{QE}$ (and its shape in Q^2_{QE}) and model predictions, expressed as χ^2 per degree of freedom (d.o.f) for eight (seven) degrees of freedom.

	Model	RFG	SuSA	RMF	EMA
ν_μ	Rate χ^2/d.o.f	1.62	2.98	2.58	2.19
	Shape χ^2/d.o.f	1.82	4.00	2.90	2.87
$\bar{\nu}_\mu$	Rate χ^2/d.o.f	3.23	3.59	3.92	3.52
	Shape χ^2/d.o.f	3.69	4.88	4.66	4.65

In Table II we present the results obtained through a χ^2 test using cross sections (rate) and fractions of cross sections (shape) for neutrinos and antineutrinos and considering the four models: SuSA, RMF, EMA, and RFG. This test allows us to estimate quantitatively the level of agreement between data and predictions, accounting for the significant correlations between the data points. Note that the fit analysis seems to work better for neutrinos and the χ^2 values are slightly smaller in the case of the rate observable. The values obtained for χ^2 indicate that there are some differences between all of the theoretical models and the data. As seen in Fig. 7, all of the models considered in this work fall below GENIE's predictions for the larger and smaller bins in Q^2_{QE}. Where experimental uncertainties are small enough to draw conclusions, the same trend appears to be seen in the data. Although not shown we have checked that the χ^2 fit improves very significantly if the lowest Q^2_{QE} value is removed from the analysis.

III. CONCLUSIONS

Summarizing, we have presented predictions for the differential cross sections corresponding to the MINERνA experiment with two nuclear models, SuSA and RMF. Both models are based on the IA and work nicely in describing QE (e, e') data. Contrary to previous studies for the MiniBooNE experiment, we have shown that the two models provide a good description of MINERνA data without the need of increasing the nucleon axial mass and without having to invoke any significant contributions from 2p2h MEC. Finally, a discussion of results for the ratios to GENIE has been also presented.

Our present studies, in addition to previous ones applied to the MiniBooNE and NOMAD experiments, seem to indicate either some inconsistency between these experiments (for example in the definition of what is "quasielastic" and what is "pion production") or that the nuclear effects that MiniBooNE appears to require vanish to a large extent at MINERνA's kinematics. With regard to the last, work is in progress aimed at extending the modeling of a relativistic 2p2h MEC analysis into the kinematical regime of MINERνA and NOMAD. Preliminary results indicate that 2p2h MEC effects might be expected to add about 12%–15% to the IA results shown in this paper, in qualitative

agreement with the findings of [21] and [26]. What is reassuring at present is that the differences between the models at the higher energy MINERνA kinematics are much smaller than for the MiniBooNE kinematics. The good agreement between the IA predictions and MINERνA data resembles a similar situation for MiniBooNE data at forward-scattering angles. On the contrary, this agreement gets lost for larger angles, which bear less weight at MINERνA kinematics.

Two additional issues have been addressed in the present study: one involves the use of kinematic cuts to elucidate the main contributions to the cross section (and showing how the high-energy MINERνA measurements are actually dominated by relatively small values of q and ω), while the other shows how Pauli blocking can be incorporated in the SuSA approach, improving the agreement at small values of Q^2_{QE}.

ACKNOWLEDGMENTS

The authors thank Laura Fields for her helpful comments and explanations on the experimental analysis. This work was partially supported by DGI (Spain) (FIS2011-28738-C02-01, FIS2011-24149, and FPA2010-17142), by the Junta de Andalucía (FQM-170, 225), by the INFN National Project MANYBODY, by the Spanish Consolider-Ingenio 2000 programmed CPAN, and in part (T. W. D.) by the U.S. Department of Energy under cooperative agreement DE-FC02-94ER40818, as well as by the Bulgarian National Science Fund under Contract No. DID-02/16-17.12.2009. G. D. M. acknowledges support from a fellowship from the Fundación Cámara (University of Sevilla). M. V. I. is grateful for the warm hospitality given by the UCM and for financial support during his stay there from the SiNuRSE action within the ENSAR European project.

[1] G. A. Fiorentini *et al.* (MINERνA Collaboration), Phys. Rev. Lett. **111**, 022502 (2013).
[2] L. Fields *et al.* (MINERνA Collaboration), Phys. Rev. Lett. **111**, 022501 (2013).
[3] A. A. Aguilar-Arevalo *et al.* (MiniBooNE Collaboration), Phys. Rev. D **81**, 092005 (2010).
[4] A. A. Aguilar-Arevalo *et al.* (MiniBooNE Collaboration), Phys. Rev. D **88**, 032001 (2013).
[5] M. Martini, M. Ericson, G. Chanfray, and J. Marteau, Phys. Rev. C **81**, 045502 (2010).
[6] J. E. Amaro, M. B. Barbaro, J. A. Caballero, T. W. Donnelly, and C. F. Williamson, Phys. Lett. B **696**, 151 (2011).
[7] J. E. Amaro, M. B. Barbaro, J. A. Caballero, and T. W. Donnelly, Phys. Rev. Lett. **108**, 152501 (2012).
[8] J. Nieves, I. Ruiz Simo, and M. J. Vicente Vacas, Phys. Lett. B **707**, 72 (2012).
[9] G. D. Megias, J. E. Amaro, M. B. Barbaro, J. A. Caballero, and T. W. Donnelly, Phys. Lett. B **725**, 170 (2013).
[10] T. W. Donnelly, J. W. Van Orden, T. De Forest Jr., and W. C. Hermans, Phys. Lett. **76B**, 393 (1978).
[11] A. De Pace, M. Nardi, W. M. Alberico, T. W. Donnelly, and A. Molinari, Nucl. Phys. **A726**, 303 (2003).
[12] J. E. Amaro, C. Maieron, M. B. Barbaro, J. A. Caballero, and T. W. Donnelly, Phys. Rev. C **82**, 044601 (2010).
[13] J. E. Amaro, M. B. Barbaro, J. A. Caballero, T. W. Donnelly, A. Molinari, and I. Sick, Phys. Rev. C **71**, 015501 (2005).
[14] J. E. Amaro, M. B. Barbaro, J. A. Caballero, T. W. Donnelly, and J. M. Udias, Phys. Rev. D **84**, 033004 (2011).
[15] C. Maieron, J. E. Amaro, M. B. Barbaro, J. A. Caballero, T. W. Donnelly, and C. F. Williamson, Phys. Rev. C **80**, 035504 (2009).
[16] R. Rosenfelder, Ann. Phys. (N.Y.) **128**, 188 (1980).
[17] C. Maieron, T. W. Donnelly, and I. Sick, Phys. Rev. C **65**, 025502 (2002).
[18] Y. Horikawa, F. Lenz, and N. C. Mukhopadhyay, Phys. Rev. C **22**, 1680 (1980).
[19] O. Benhar, P. Coletti, and D. Meloni, Phys. Rev. Lett. **105**, 132301 (2010).
[20] J. M. Udias, P. Sarriguren, E. Moya de Guerra, E. Garrido, and J. A. Caballero, Phys. Rev. C **48**, 2731 (1993).
[21] R. Gran, J. Nieves, F. Sanchez, and M. J. Vicente Vacas, Phys. Rev. D **88**, 113007 (2013).
[22] W. M. Alberico, A. Molinari, T. W. Donnelly, E. L. Kronenberg, and J. W. Van Orden, Phys. Rev. C **38**, 1801 (1988).
[23] C. Andreopoulos (GENIE Collaboration), Acta Phys. Pol. B **40**, 2461 (2009).
[24] T. Golan, C. Juszczak, and J. T. Sobczyk, Phys. Rev. C **86**, 015505 (2012).
[25] Jesse Chvojka, Ph.D. Dissertation, University of Rochester, 2012.
[26] U. Mosel, O. Lalakulich, and K. Gallmeister, arXiv:1402.0297.